# Newmark-Beta Method in Discrete Elastic Rods Algorithm to Avoid Energy Dissipation

**Weicheng Huang**
Department of Mechanical and Aerospace Engineering,
University of California, Los Angeles,
Los Angeles, CA 90095
e-mail: weichengh1995@g.ucla.edu

**Mohammad Khalid Jawed**[1]
Department of Mechanical and Aerospace Engineering,
University of California, Los Angeles,
Los Angeles, CA 90095
e-mail: khalidjm@seas.ucla.edu

*Discrete elastic rods (DER) algorithm presents a computationally efficient means of simulating the geometrically nonlinear dynamics of elastic rods. However, it can suffer from artificial energy loss during the time integration step. Our approach extends the existing DER technique by using a different time integration scheme—we consider a second-order, implicit Newmark-beta method to avoid energy dissipation. This treatment shows better convergence with time step size, specially when the damping forces are negligible and the structure undergoes vibratory motion. Two demonstrations—a cantilever beam and a helical rod hanging under gravity—are used to show the effectiveness of the modified discrete elastic rods simulator.* [DOI: 10.1115/1.4043793]

## 1 Introduction

Recent activities in the field of discrete differential geometry (DDG) have fueled the development of simple, robust, and efficient tools for physics-based simulations of slender elastic structures in the computer graphics community [1–4]. The DDG-based simulations begin with a physical model that is discretized from the ground up such that the key geometric structures representing the actual smooth physical system of preserved [5]. One of the important applications of DDG in physics-based modeling is discrete elastic rods (DERs) method [3,4] for capturing the geometrically nonlinear deformation of thin elastic rods, e.g., curly hairs. Their deformations are characterized by stretching, bending, and twisting on the basis of the Kirchhoff's rod theory [6,7]. Stretching and bending are captured by the deformation of a curve called the centerline, while twisting is formulated by the rotation of a material frame associated with each segment on the centerline [3]. Recently, DER has been embraced by the mechanics community, and excellent agreement has been found between DER-based simulations and physical experiments [8–11].

However, the first-order Euler integration (implicit on elastic and explicit on external forces) used in original DER algorithm is not physically accurate when simulating structural dynamics in low damping environment, because of the energy dissipation induced by this nonsymplectic time integration. This issue was not observed in previous DER-based investigations. Some of these studies focused on static [11] or quasi-static deformations [8] and ignored the inertial dynamics. In other studies, the damping force was predominant, and vibratory motions were absent [9,10]. As a result, the energy loss of Euler integration was negligible. However, when studying the fast dynamic response of slender structures, e.g., shape memory alloy-based actuator in soft robotics engineering [12–14], inertial dynamics is prominent and the numerical error caused by artificial energy dissipation is no longer acceptable. This inspires us to consider a different time marching technique based on the second-order Newmark-beta method to maintain energy conservation [15–18].

In this technical brief, we augment DER simulation by a second-order time integration method—Newmark-beta method—to better capture the geometrically nonlinear dynamics of elastic rods. Although the previous studies focused on simulating the static/quasi-static deformations and damping-dominated dynamics, here, we focus on structural dynamics where inertia is preponderant and environmental damping is absent. We use two examples—a cantilever beam and a naturally helical rod hanging under gravity—to demonstrate the advancements of this Newmark-beta-based DER algorithm over the original formulation.

## 2 Methodology

In the discrete setting of DER shown schematically in Fig. 1(*a*), the rod centerline is discretized into $N$ nodes: $\mathbf{x}_0, \ldots, \mathbf{x}_{N-1}$, which corresponds to $N-1$ edge vectors: $\mathbf{e}^0, \ldots, \mathbf{e}^{N-2}$ such that $\mathbf{e}^i = \mathbf{x}_{i+1} - \mathbf{x}_i$ and $i = 0, \ldots, N-2$. Hereafter, we use subscripts to denote quantities associated with the nodes, e.g., $\mathbf{x}_i$, and superscripts when associated with edges, e.g., $\mathbf{e}^i$. Each edge, $\mathbf{e}^i$, has an orthonormal adapted reference frame $\{\mathbf{d}_1^i, \mathbf{d}_2^i, \mathbf{t}^i\}$ and a material frame $\{\mathbf{m}_1^i, \mathbf{m}_2^i, \mathbf{t}^i\}$; both the frames share the tangent $\mathbf{t}^i = \mathbf{e}^i/|\mathbf{e}^i|$ as one of the directors. The reference frame is updated at each time step through parallel transport in time, and referring to Fig. 1(*b*), the material frame can be obtained from a scalar twist angle $\theta^i$. See Ref. [19] for a detailed exposition of the DER algorithm. Node positions together with twist angles constitute the $4N-1$-sized degrees of freedom (DOF) vector $\mathbf{q} = [\mathbf{x}_0, \theta^0, \mathbf{x}_1, \ldots, \mathbf{x}_{N-2}, \theta^{N-2}, \mathbf{x}_{N-1}]$ of the discrete rod. Based on this kinematic representation, in the remainder of this section, we discuss the formulation of elastic energies, elastic forces, and the time-stepping procedure of the rod solver.

An elastic rod is modeled as a mass-spring system, with a lumped mass (and angular mass) at each node (and edge), and associated discrete stretching, bending, and twisting energies. For a rod with Young's modulus $E$, shear modulus $G$, and isotropic circular cross section, the elastic energies—stretching, bending, and twisting—are given by [3,4]

$$E_s = \frac{1}{2}\sum_{i=0}^{N-2} EA(\boldsymbol{\varepsilon}^i)^2 |\bar{\mathbf{e}}^i| \tag{1a}$$

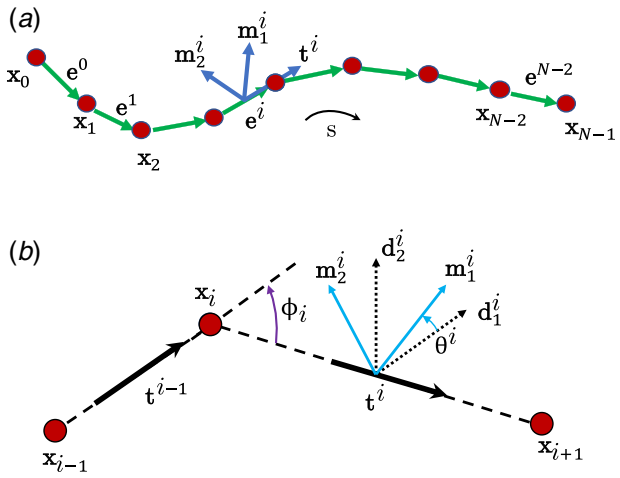


**Fig. 1 (*a*) Discrete schematic diagram of a rod and (*b*) notations used in our discrete model. Bending curvature is related to turning angle, $\kappa_i = 2\tan(\phi_i/2)$**

[1]Corresponding author.

Contributed by the Applied Mechanics Division of ASME for publication in the Journal of Applied Mechanics. Manuscript received April 8, 2019; final manuscript received May 13, 2019; published online June 4, 2019. Assoc. Editor: Caglar Oskay.

  

$$E_b = \frac{1}{2}\sum_{i=0}^{N-1}\frac{EI}{\Delta l_i}\left[(\kappa_i^{(1)} - \bar{\kappa}_i^{(1)})^2 + (\kappa_i^{(2)} - \bar{\kappa}_i^{(2)})^2\right] \tag{1b}$$

$$E_t = \frac{1}{2}\sum_{i=0}^{N-1}\frac{GJ}{\Delta l_i}(\tau_i)^2 \tag{1c}$$

where $A$ is the area of cross section, $I$ is the area moment of inertia, $J$ is the polar moment of inertia, $\varepsilon^i$ is the stretching strain associated with the $i$th edge, $\bar{\mathbf{e}}^i$ is its undeformed length, $\kappa_i^{(1)}$ and $\kappa_i^{(2)}$ are the bending curvatures at the $i$th node ($\bar{\kappa}_i^{(1)}$ and $\bar{\kappa}_i^{(2)}$ are the curvatures in the undeformed configuration), $\tau_i$ is the twist at the $i$th node, and $\Delta l_i = (|\mathbf{e}^i| + |\mathbf{e}^{i+1}|)/2$ is its Voronoi length. The strain measures, i.e., $\varepsilon^i$, $\kappa_i^{(1)}$, $\kappa_i^{(2)}$, and $\tau_i$, can be expressed in terms of $\mathbf{q}$ (specifically, $\mathbf{x}_{i-1}$, $\theta^{i-1}$, $\mathbf{x}_i$, $\theta^i$, $\mathbf{x}_{i+1}$). The case of noncircular cross-section can be included in the above formulation with minor changes [3,4].

At each degree of freedom $q_j$, the elastic forces (associated with nodal positions) and elastic moments (associated with the twist angles) are

$$F_j^{\text{int}} = -\frac{\partial}{\partial q_j}(E_s + E_b + E_t) \tag{2}$$

where $j$ is an integer between 0 and $4N-2$.

The system of equations of motion is

$$\mathbf{M}\ddot{\mathbf{q}} = \mathbf{F}^{\text{int}} + \mathbf{F}^{\text{ext}} \tag{3}$$

where $\mathbf{F}^{\text{ext}}$ is the external force vector (e.g., gravity and damping force), $\mathbf{M}$ is the diagonal mass matrix composed of the lumped masses, and $\dot{()}$ represents derivative with respect to time. In the discrete time-stepping scheme of the original DER method, implicit Euler integration is used to solve the following $4N-1$ equation of motions and update the DOF vector $\mathbf{q}$ and its velocity (time derivative of DOF) $\mathbf{v} = \dot{\mathbf{q}}$ from time step $t_k$ to $t_{k+1} = t_k + h$ ($h$ is the time step size):

$$\mathbf{M}\Delta\mathbf{q}_{k+1} - h\mathbf{M}\mathbf{v}_k - h^2\left(\mathbf{F}_{k+1}^{\text{int}} + \mathbf{F}_{k+1}^{\text{ext}}\right) = 0 \tag{4a}$$

$$\mathbf{q}_{k+1} = \mathbf{q}_k + \Delta\mathbf{q}_{k+1} \tag{4b}$$

$$\mathbf{v}_{k+1} = \frac{1}{h}\Delta\mathbf{q}_{k+1} \tag{4c}$$

where subscript $k+1$ (and $k$) denotes evaluation of the quantity at time $t_{k+1}$ (and $t_k$). The Jacobian associated with Eq. (4a) is necessary for Newton's iteration and can be expressed as

$$\mathbb{J}_{ij} = m_i\delta_{ij} - h^2\left(-\frac{\partial^2(E_s + E_b + E_t)}{\partial q_i \partial q_j} + \frac{\partial F_i^{\text{ext}}}{\partial q_j}\right) \tag{5}$$

where $i$ and $j$ are integers between 0 and $4N-2$, the mass (or angular mass) associated with the $i$th DOF is $m_i$, the energies ($E_s$, $E_b$, $E_t$) are evaluated at $t = t_{k+1}$, and $F_i^{\text{ext}}$ is the $i$th element of the vector $\mathbf{F}_{k+1}^{\text{ext}}$. If the gradient of the external force vector $\left(\partial F_i^{\text{ext}}/\partial q_j\right)$ cannot be analytically evaluated, this term is often neglected, i.e., external forces are treated explicitly. Importantly, the Jacobian $\mathbb{J}$ is a banded matrix and the time complexity of this algorithm is $O(N)$, i.e., the computational time linearly scales with the number of nodes [4]. This computational efficiency has motivated its application in the animation industry (e.g., hair simulation for movies) as well as its adoption in mechanical engineering.

This first-order time integration can cause energy dissipation in long-time dynamic simulations, because the time stepping from $t_k$ to $t_{k+1}$ is treated as a constant speed process and the effect of acceleration is partially ignored. Here, we modify the time integrating algorithm by a second-order, implicit Newmark-beta update [17] such that

$$\begin{aligned}\mathbf{M}\Delta\mathbf{q}_{k+1} - h\mathbf{M}\mathbf{v}_k - h^2\beta(1-\beta)\left(\mathbf{F}_{k+1}^{\text{int}} + \mathbf{F}_{k+1}^{\text{ext}}\right)\\ - h^2\beta^2\left(\mathbf{F}_k^{\text{int}} + \mathbf{F}_k^{\text{ext}}\right) = \mathbf{0}\end{aligned} \tag{6a}$$

$$\mathbf{q}_{k+1} = \mathbf{q}_k + \Delta\mathbf{q}_{k+1} \tag{6b}$$

$$\mathbf{v}_{k+1} = \frac{1}{h\beta}\Delta\mathbf{q}_{k+1} - \frac{1-\beta}{\beta}\mathbf{v}_k \tag{6c}$$

where $\beta$ is a parameter between 0.5 and 1.0. At $\beta = 0.5$, the acceleration of the DOFs at the current time step $t = t_{k+1}$ is computed based on the mean of applied forces (elastic and external) evaluated at $t = t_k$ and $t = t_{k+1}$. We expect the numerical energy dissipation to disappear at this value of $\beta$, as evidenced in Sec. 3. Also note that when $\beta = 1.0$, Eqs. (6) reduce to Eqs. (4). The Jacobian matrix of Eqs. (6) is

$$\mathbb{J}_{ij} = m_i\delta_{ij} - h^2\beta(1-\beta)\left(-\frac{\partial^2(E_s + E_b + E_t)}{\partial q_i \partial q_j} + \frac{\partial F_i^{\text{ext}}}{\partial q_j}\right) \tag{7}$$

such that Eqs. (6) can be solved using Newton's iterations, similar to Eqs. (4). The banded nature of the Jacobian matrix and the $O(N)$ time complexity are maintained.

## 3 Results

In this section, we compare the original DER algorithm (Euler integration) and the updated method (Newmark-beta update) using two examples. We specifically focus on the energy dissipation and the dependence of the solution on the time step size $h$. In the first example shown in Fig. 2(a), consider a cantilever beam hanging under gravity with the following physical parameters: rod length $L = 0.5$ m, cross-sectional radius $r_0 = 0.5$ cm, (with

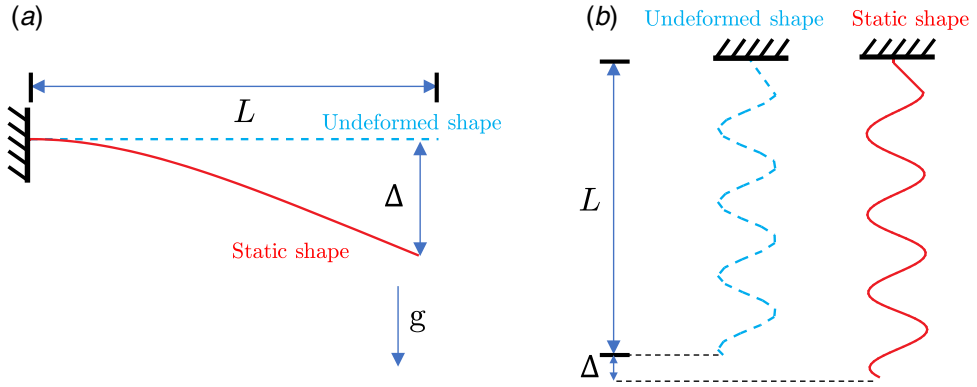


**Fig. 2 Shape of the rod in two demonstrations: (*a*) cantilever beam and (*b*) helical rod**

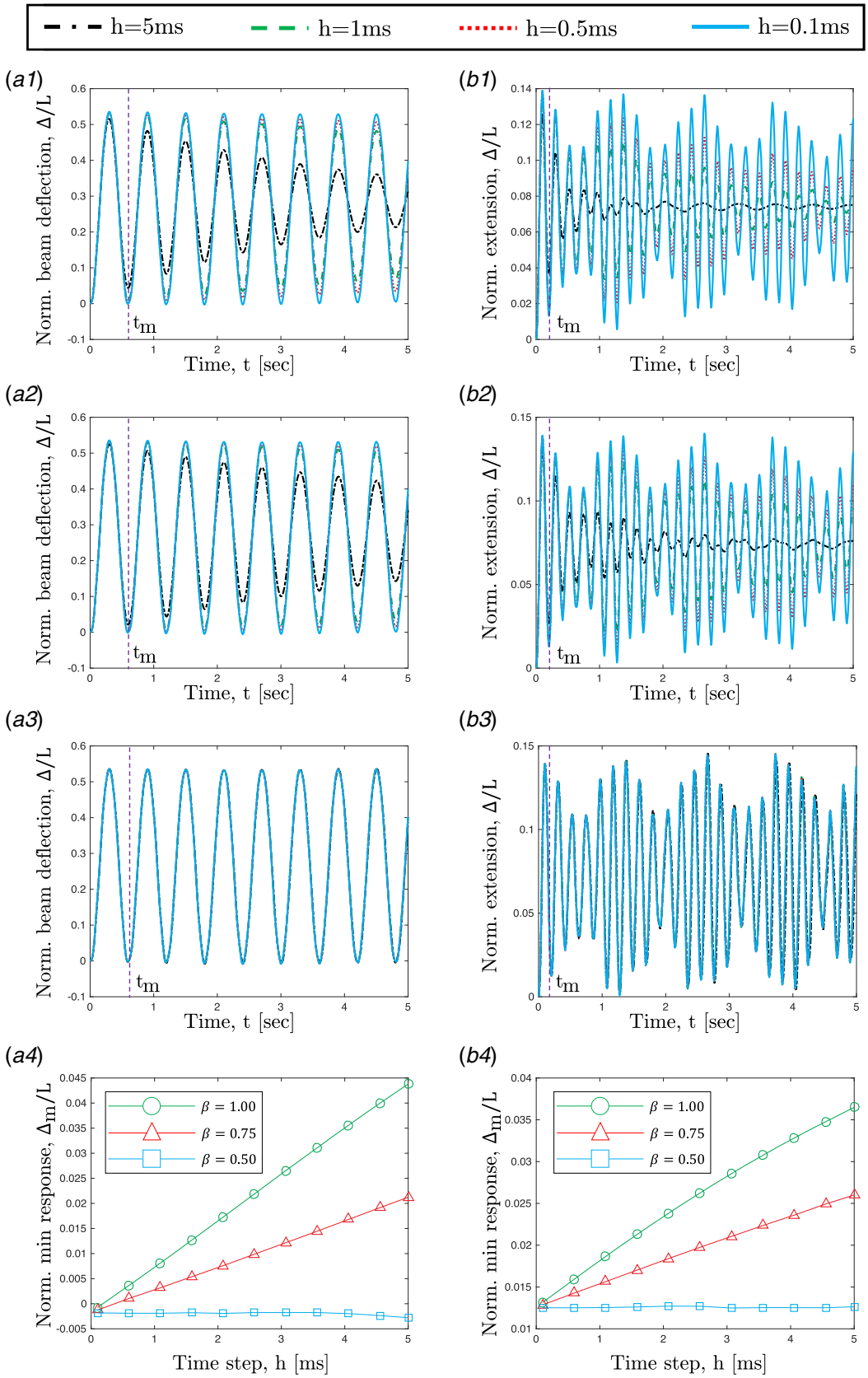


**Fig. 3 Comparison between Euler method and Newmark-beta method for (*a*) a cantilever beam and (*b*) a helix. From (1) to (4): (1) Euler method (β = 1.0); (2) Newmark-beta method with β = 0.75; (3) Newmark-beta method with β = 1.0; and (4) normalized minimum deflection $\Delta_m/L$ in the first cycle as a function of time step size *h*. Here, $\Delta_m$ is the first local minimum displacement (at time $t = t_m$) for $t > 0$**

moment of inertia $I = \pi r_0^4/4$ and cross-sectional area $A = \pi r_0^2$), Young's modulus $E = 0.1$ GPa, shear modulus $G = E/3$ (i.e., incompressible material with Poisson's ratio $\nu = 0.5$), density $\rho = 1273.52$ kg/m$^3$, and acceleration due to gravity, $g = 9.8$ m/s$^2$; the density and elastic moduli are similar to the experimental rods used in Ref. [8]. Figure 3(*a*1) shows the normalized tip deflection $\Delta/L$ as a function of time using the original DER method (Eqs. (4)). The beam undergoes a vibratory motion, and the amplitude of the deflection decreases with the time step size $h$. At $h = 5$ ms, the amplitude reduces to one-third of the initial amplitude within 5 s. Eventually, the amplitude reduces to zero, and the final static configuration has $\Delta/L \approx 0.3$. At smaller values of $h$, the decay time is larger; nonetheless, after a sufficiently long time, the final configuration is static regardless of $h$ and is shown in Fig. 2(*a*) using a solid line. This is a direct result of the energy dissipation caused by the time-stepping procedure. Since there is no damping force present in the example, the beam should maintain a pendulum-like periodic motion for an infinite time.

In order to remedy this issue, we consider Newmark-beta-based modified DER (Eqs. (6)) in Figs. 3(*a*2) and 3(*a*3) and plot the tip deflection with time. The energy dissipation is reduced at $\beta = 0.75$, and the motion is periodic without noticeable decay in amplitude for $\beta = 0.5$. We verified that the sum of kinetic and potential (elastic and gravitational) energies remains unchanged with time in all the cases considered in Fig. 3(*a*3). For a direct comparison between the two methods, Fig. 3(*a*4) shows the minimum tip deflection in the first cycle $\Delta_m$ (i.e., deflection at $t = t_m$, where $t_m$ is shown in Figs. 3(*a*2) and 3(*a*3)) as a function of $h$. While $\Delta_m$ increases almost linearly with $h$ for $\beta = 1$ (used in the original DER method) and $\beta = 0.75$. However, the amount of dissipation is reduced by changing $\beta$ from 1.0 to 0.75. When $\beta = 0.5$, the modified method shows no dependence on $h$ as long as $h \lesssim 3$ ms. In summary, the modified algorithm resolves the issue with energy loss, allows larger time step size while retaining the physics of the system, and, therefore, improves the computation time.

In the second demonstration shown schematically in Fig. 2(*b*), a naturally helical rod is hanging under gravity, with helix radius $R = 2$ cm, pitch $\lambda = 5$ cm, contour length $s = 0.5$ m (resulting in an axial length $L \approx 0.185$ m), and Young's modulus $E = 10$ MPa. The other parameters ($\rho$, $g$, $\nu$) remain unchanged from the previous cantilever beam example. Figures 3(*b*1)–3(*b*3) show the normalized tip extension $\Delta/L$ (see Fig. 2(*b*) for a schematic of $\Delta$) with time at different values of $h$ using the original DER method and the modified one. In this example, we again notice that the original method sees energy dissipation (and a decay in the amplitude of the motion) as well as strong dependence on the time step size. The modified approach with $\beta = 0.5$, on the other hand, again remedies both of these two issues. Figure 3(*b*4) presents the normalized minimum extension in the first cycle $\Delta_m/L$ versus the time step size $h$ for different values of $\beta$ and affirms that the Newmark-beta-based DER shows better convergence with time step size.

We should note that, despite the lack of accuracy in capturing the physics of the problems, the Euler method-based DER, aided by artificial energy dissipation, can stably take larger time step size [20]. In both the model cases presented above, this method runs into numerical instability in Newton's iterations at $h \gtrsim 100$ ms. However, the second-order integration method in DER necessitates $h \lesssim 10$ ms for stable simulation. This difference in the maximum stable step size decreases when damping, e.g., an external force proportional and opposite to velocity, is introduced. As damping resists velocity, such force prevents large changes in nodal coordinates within a single time step and thus typically improves the numerical stability of the algorithm. In short, if fast and stable simulation is the primary concern and the accurate description of the physics is not essential, the original DER formulation with large time step size should be chosen. On the other hand, if accurate dynamics is the focus, the modified Newmark-beta-based DER algorithm should be chosen.

## 4 Concluding Remarks

We showed the artificial energy dissipation, using two examples, in the original DER method based on Euler integration and demonstrated that a second-order time integration method can solve this issue. Moreover, the modified method shows superior performance when considering the simulation result with a time step size. In the future, other high-order time integration methods, e.g., Range–Kutta method, can be considered. It will be of value to study the implication of the choice of integration method on the accuracy and stability of the DER method. Since our ultimate goal for this technical brief is to resolve the artificial energy dissipation (e.g., for simulation of dynamics of soft robots), we are satisfied with this second-order, Newmark-beta method with $\beta = 0.5$. This extension can now allow DER to seamlessly capture inertia-dominated dynamic processes.


## Funding Data

- Henry Samueli School of Engineering and Applied Science, University of California, Los Angeles (Funder ID: 10.13039/100007185).


## References


[1] Baraff, D., and Witkin, A., 1998, "Large Steps in Cloth Simulation," Proceedings of the 25th Annual Conference on Computer Graphics and Interactive Techniques, Orlando, FL, July 19–24, ACM, pp. 43–54.

[2] Grinspun, E., Hirani, A. N., Desbrun, M., and Schröder, P., 2003, "Discrete Shells," Proceedings of the 2003 ACM SIGGRAPH/Eurographics Symposium on Computer Animation, San Diego, CA, July 27–31, Eurographics Association, pp. 62–67.

[3] Bergou, M., Wardetzky, M., Robinson, S., Audoly, B., and Grinspun, E., 2008, "Discrete Elastic Rods," ACM Trans. Graphics (TOG), **27**(3), p. 63.

[4] Bergou, M., Audoly, B., Vouga, E., Wardetzky, M., and Grinspun, E., 2010, "Discrete Viscous Threads," ACM Trans. Graphics (TOG), **29**(4), p. 116.

[5] Grinspun, E., Desbrun, M., Polthier, K., Schröder, P., and Stern, A., 2006, "Discrete Differential Geometry: An Applied Introduction," ACM SIGGRAPH Course, **7**, pp. 1–139.

[6] Kirchhoff, G., 1859, "Uber Das Gleichgewicht Und Die Bewegung Eines Unendlich Dunnen Elastischen Stabes," J. Reine Angew. Math., **1859**(56), pp. 285–313.

[7] Audoly, B., and Pomeau, Y., 2010, *Elasticity and Geometry: From Hair Curls to the Non-linear Response of Shells*, Oxford University Press, Oxford.

[8] Jawed, M. K., Da, F., Joo, J., Grinspun, E., and Reis, P. M., 2014, "Coiling of Elastic Rods on Rigid Substrates," Proc. Natl. Acad. Sci. U. S. A., **111**(41), pp. 14663–14668.

[9] Jawed, M. K., Khouri, N. K., Da, F., Grinspun, E., and Reis, P. M., 2015, "Propulsion and Instability of a Flexible Helical Rod Rotating in a Viscous Fluid," Phys. Rev. Lett., **115**(16), p. 168101.

[10] Jawed, M. K., and Reis, P. M., 2017, "Dynamics of a Flexible Helical Filament Rotating in a Viscous Fluid Near a Rigid Boundary," Phys. Rev. Fluids, **2**(3), p. 034101.

[11] Baek, C., Sageman-Furnas, A. O., Jawed, M. K., and Reis, P. M., 2018, "Form Finding in Elastic Gridshells," Proc. Natl. Acad. Sci. U. S. A., **115**(1), pp. 75–80.

[12] Huang, X., Kumar, K., Jawed, M. K., Nasab, A. M., Ye, Z., Shan, W., and Majidi, C., 2018, "Chasing Biomimetic Locomotion Speeds: Creating Untethered Soft Robots With Shape Memory Alloy Actuators," Sci. Rob., **3**(25), p. eaau 7557.

[13] Huang, X., Kumar, K., Jawed, M. K., Mohammadi, Nasab, Shan, W., and Majidi, C., 2019, "Highly Dynamic Shape Memory Alloy Actuator for Fast Moving Soft Robots," Adv. Mater. Technol., p. 1800540.

[14] Huang, X., Kumar, K., Jawed, M. K., Ye, Z., and Majidi, C., 2019, "Soft Electrically Actuated Quadruped (SEAQ)-Integrating a Flex Circuit Board and Elastomeric Limbs for Versatile Mobility," IEEE Rob. Autom. Lett., **4**(3), pp. 2415–2422.

[15] Hughes, T. J., 2012, *The Finite Element Method: Linear Static and Dynamic Finite Element Analysis*, Courier Corporation, North Chelmsford, MA.

[16] Skouras, M., Thomaszewski, B., Coros, S., Bickel, B., and Gross, M., 2013, "Computational Design of Actuated Deformable Characters," ACM Trans. Graphics (TOG), **32**(4), p. 82.

[17] Chen, D., Levin, D. I., Matusik, W., and Kaufman, D. M., 2017, "Dynamics-aware Numerical Coarsening for Fabrication Design," ACM Trans. Graphics (TOG), **36**(4), p. 84.

[18] Shen, Z., Huang, J., Chen, W., and Bao, H., 2015, *Computer Graphics Forum*, Vol. 34, Hoboken, NJ, pp. 145–154.

[19] Jawed, M. K., Novelia, A., and O'Reilly, O. M., 2018, *A Primer on the Kinematics of Discrete Elastic Rods*, Springer, New York.

[20] Hahn, G., 1991, "A Modified Euler Method for Dynamic Analyses," Int. J. Numer. Methods Eng., **32**(5), pp. 943–955.